

# Uneven Error Ellipsoid-Based Model Predictive Control for Planetary Safe Landings

Dantong Ge\* Pingyuan Cui\* Shengying Zhu\* Zixuan Liang\*

\* Beijing Institute of Technology, Beijing, China 100081 (e-mail:  
gedt@bit.edu.cn, cuiipy@bit.edu.cn, zhushy@bit.edu.cn,  
liangzx@bit.edu.cn).

---

**Abstract:** Considering the impact of both position and velocity estimate errors on hazard avoidance, this paper proposes an uneven error ellipsoid-based model predictive control for planetary landing missions. The uneven error ellipsoid model not only takes into account system position uncertainty at the moment, but also reflects how fast the system is approaching the nearby hazard in the position space. By repetitively computing the current space margin and the most dangerous direction, the system quantifies the threat posed by the environment as the lander descends to the surface. In order to perform a safe and precise landing, we apply model predictive control during descent and incorporate a hazard avoidance performance index into the problem. Then, we validate the proposed method in a Bennu-based asteroid landing scenario and demonstrate its effectiveness of improving landing safety.

*Keywords:* Autonomous system; Model predictive control; Hazard avoidance; State uncertainty; Landing safety

---

## 1. BACKGROUND

Performing a safe and precise landing on the planetary surface is technically challenging. Due to environment disturbances and modeling errors, the actual state of the system may not strictly follow the trajectory planned under nominal conditions. Besides, large boulders and rocks on the surface may pose collision threats to the lander when it gets close to the target Cui et al. (2018). To ensure landing safety, future planetary exploration missions favor an enhanced onboard autonomy for generating reliable real-time trajectories on the basis of current state estimates and environment measurements Ge et al. (2019).

For constrained planetary safe landing problems, model predictive control (MPC) makes a promising methodology to be applied, as it is able to handle both control objectives and hard constraints in a unified framework Liao-McPherson et al. (2016); Reynolds and Mesbahi (2017). One of the most important objectives to be accounted in the landing process is hazard avoidance. To this end, methods that incorporate exclusion constraints or glide-slope constraints into trajectory optimization are discussed in the literature Lee and Mesbahi (2017). In Park et al. (2016), the spacecraft realizes hazard avoidance by incorporating rotating and fixed hyperplane constraints into receding horizon optimization problems. It is proved that directly implementing nonlinear avoidance constraints would lead to an improved performance with regard to time or fuel-consumption, compared to the case with approximated convex constraints. It, however, may bring difficulties in problem solving and solution convergence Jewison et al. (2015). Considering the influence of non-convex constraints on problem solving efficiency,

techniques of linearization, affine approximation, lossless convexification, and successive convexification are developed Reynolds and Mesbahi (2017); Szmuk et al. (2016). Nevertheless, these available hazard avoidance methods are mainly developed on the basis of accurate system state estimates. In real missions, the onboard navigation outputs may not be consistent with the actual system states due to modeling errors and measurement noises Lindner et al. (2010). To account for navigation uncertainties in trajectory design, Yuan et al. (2018) proposes a probability-based hazard avoidance guidance method. By minimizing the obstacle collision probability posed by position uncertainties, the method derives an analytical guidance law using Lyapunov's theorem.

Apart from position uncertainties, the velocity that the system is approaching the hazard also matters in hazard avoidance. For example, for a fixed distance to the hazard, system safety is more challenged if the lander is moving at a higher speed. Motivated by this, the paper incorporates system velocity and its estimate errors in trajectory optimization and proposes an uneven error ellipsoid-based hazard avoidance method.

## 2. PROBLEM STATEMENT

Assume that the system dynamics can be approximated by a linear time-invariant system around the current system state through dynamic state feedback

$$\mathbf{x}(k+1) = \mathbf{A}\mathbf{x}(k) + \mathbf{B}\mathbf{u}(k) + \mathbf{d}(k) \quad (1)$$

where  $\mathbf{x} \in \mathcal{X}$  is the system state,  $\mathbf{u} \in \mathcal{U}$  is the control action, and  $\mathbf{d} \in \mathcal{D}$  is the modeling error resulted from environment disturbances and dynamics linearization. Given the initial state  $\mathbf{x}_0$  and the targeted state  $\mathbf{x}_f$ , a physically

feasible trajectory is to be planned to deliver the lander from the current position to the assigned landing site. Denote the hazard set by  $\mathcal{O}$ . For landing safety, the system should keep a safe distance away from these hazards.

During descent, the system makes onboard decisions based on real-time state estimates. Denote the actual system state as  $\mathbf{x}_a = [\mathbf{r}_a^T, \mathbf{v}_a^T]^T$ , and the estimated system state as  $\mathbf{x}_e = [\mathbf{r}_e^T, \mathbf{v}_e^T]^T$ . Here, we assume that both position and velocity estimates generated from the navigation module follow Gaussian distribution. The mean value of system position estimate is  $\boldsymbol{\mu}_r$  and its covariance is  $C_r$ . The mean value of system velocity estimate is  $\boldsymbol{\mu}_v$  and its covariance is  $C_v$ . Hence, it holds that  $\mathbf{r}_e = \boldsymbol{\mu}_r$ ,  $\mathbf{v}_e = \boldsymbol{\mu}_v$ . Considering the impact of state estimate errors on hazard avoidance and landing performance, we formulate the following problem

*Problem 1: Let the system dynamics be governed by Eq. 1. Let the initial and terminal state  $\mathbf{x}_0, \mathbf{x}_f \in \mathcal{X}$ , the feasible control set  $\mathcal{U}$ , and the detected hazard set  $\mathcal{O}$  be given. Assume that the system position and velocity estimates satisfy  $\mathbf{r}_e \sim N(\boldsymbol{\mu}_r, C_r)$ ,  $\mathbf{v}_e \sim N(\boldsymbol{\mu}_v, C_v)$ . Let  $T > 0$  be the duration of the landing process. For a designated landing error  $\varepsilon$ , find a control signal  $u^* : [0, T] \rightarrow \mathcal{U}$  that satisfies the following conditions for all  $t \in [0, T]$ :*  
 (1)  $\|\mathbf{x}_a(T) - \mathbf{x}_f\| \leq \varepsilon$ ;  
 (2) the actual system position  $\mathbf{r}_a(t) \notin \mathcal{O}$ .

### 3. METHODOLOGY

#### 3.1 Uneven error ellipsoid model

According to the navigation results, we use a  $3\sigma$  position error ellipsoid around  $\boldsymbol{\mu}_r$  to bound the actual position of the system. Define the ellipsoid coordinate system (c.s.) centered around  $\boldsymbol{\mu}_r$  as  $\mathcal{F}_E$ . The axes of the coordinate system coincide with the three axes of the  $3\sigma$  position error ellipsoid. We can then transform the covariance matrix  $C_r$  from the target-fixed c.s.  $\mathcal{F}$  to the ellipsoid c.s.  $\mathcal{F}_E$  by

$$U_E^T C_r U_E = D \quad (2)$$

where  $D$  is a diagonal matrix whose non-zero elements are the eigenvalues of matrix  $C_r$ . The orthogonal matrix  $U_E$  is the transformation matrix from the target-fixed c.s.  $\mathcal{F}$  to the ellipsoid c.s.  $\mathcal{F}_E$ , whose columns are the eigenvectors of matrix  $C_r$ . Denote the system's position vector in the target-fixed c.s. as  $\mathbf{r}$  and in the ellipsoid c.s. as  $\mathbf{r}^E$ . It holds that

$$\mathbf{r}^E = U_E^T (\mathbf{r} - \mathbf{r}_e) \quad (3)$$

and the actual position of the system

$$\frac{1}{9} (\mathbf{r}^E)^T D^{-1} \mathbf{r}^E \leq 1 \quad (4)$$

Here, we sample  $M_r$  points from the position space that satisfies inequality (4), which constitute set  $\mathcal{S}_r$

$$\mathcal{S}_r = \{\mathbf{r}_i | \frac{1}{9} (\mathbf{r}_i^E)^T D^{-1} \mathbf{r}_i^E \leq 1, i = 1, \dots, M_r\} \quad (5)$$

Note that the number of sample points should not be too small to represent the position distribution characteristics, nor should it be too large to go beyond system online processing ability.

Then, we expand the ellipsoid according to the velocity estimate errors. Based on the velocity estimate covariance matrix  $C_v$ , we obtain the variance at each direction

$$\text{diag}(C_v) = \begin{bmatrix} \sigma_{vx}^2 & 0 & 0 \\ 0 & \sigma_{vy}^2 & 0 \\ 0 & 0 & \sigma_{vz}^2 \end{bmatrix} \quad (6)$$

where  $\boldsymbol{\sigma}_v = [\sigma_{vx}, \sigma_{vy}, \sigma_{vz}]^T$  are the standard deviations of the velocity estimate in the target-fixed c.s.  $\mathcal{F}$ . Here we consider the distance that the system can reach when no control is applied in  $\Delta T$ . Although a more robust formulation could be established by taking all possible control actions into account, we focus on predictions without control in this paper and discuss the case with control in future work. Similarly, we take  $M_v$  sample points that follow Gaussian distribution  $N(\boldsymbol{\mu}_v, \boldsymbol{\sigma}_v)$ . For any  $\mathbf{v}_i \sim N(\boldsymbol{\mu}_v, \boldsymbol{\sigma}_v)$ ,  $i = 1, \dots, M_v$ , compute

$$\Delta \mathbf{r}_i = \mathbf{v}_i \Delta T \quad (7)$$

The distance increment of each sample constitutes set  $\mathcal{S}_v$

$$\mathcal{S}_v = \{\mathbf{r} | \Delta \mathbf{r}_1, \dots, \Delta \mathbf{r}_{M_v}\} \quad (8)$$

Then, we obtain the uneven error ellipsoid set  $\mathcal{S}_E$  by conducting a Minkowski sum of the established sets

$$\mathcal{S}_E = \mathcal{S}_r \oplus \mathcal{S}_v \quad (9)$$

By defining the boundary of position uncertainty and predicting the range that the system would travel, the model reflects both position and velocity estimate errors in the position space for collision risk assessment.

#### 3.2 Real-time trajectory generation

During descent, the system obtains environment measurements from onboard sensors such as optical camera and Lidar Dunham et al. (2002). Here, we use a circumscribed sphere of every hazard to describe the areas that the system is not allowed to enter. Denote the detected hazard set by

$$\mathcal{H} = \{[x_{h1}, y_{h1}, z_{h1}, R_{h1}], \dots, [x_{hk}, y_{hk}, z_{hk}, R_{hk}], \dots\}$$

where  $[x_{hk}, y_{hk}, z_{hk}]$  is the center of the sphere and  $R_{hk}$  is its radius. In the following, we focus on landing scenarios with a single hazard, i.e.,  $\mathcal{H} = \{[x_h, y_h, z_h, R_h]\}$ , and discuss possible extensions to multi-hazard scenarios.

We adopt two variables for evaluating the actual threat that the environment poses to the lander, that is, the current space margin and the most dangerous direction. We denote the current space margin by  $d$  and use it to quantify the dynamically changing distance from the system to the nearest hazard under state uncertainties. Then, we denote the most dangerous direction by  $\mathbf{d}_0$ , which indicates the direction that system safety is most challenged. Based on the established uneven error ellipsoid model, we can update these variables as the lander descends to the target. As illustrated in Fig. 1, in the uneven error ellipsoid  $\mathcal{S}_E$ , assume that point  $p$  is the point closest to the hazard. By searching point  $p$ 's position  $\mathbf{r}_p$  on the uneven error ellipsoid surface, we calculate the current space margin by

$$d = \|\mathbf{r}_h - \mathbf{r}_p\| - R_h \quad (10)$$

where  $\mathbf{r}_h = [x_h, y_h, z_h]^T$  is the center of the hazard sphere and  $R_h$  is the radius. When there is more than one hazard to be considered, we compute the distance from the uneven error ellipsoid surface to every nearby hazard and find point  $p$  that has the minimal distance. Denote the corresponding hazard by  $[x_h^*, y_h^*, z_h^*, R_h^*]$ , and we obtain the current space margin from

$$d = \|\mathbf{r}_h^* - \mathbf{r}_p\| - R_h^* \quad (11)$$

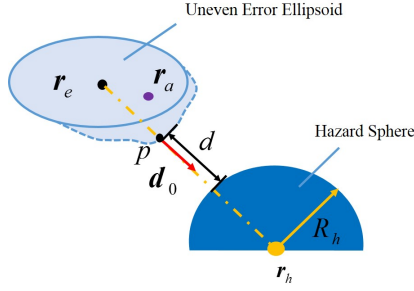


Fig. 1. Current space margin  $d$  and the most dangerous direction  $\mathbf{d}_0$ .

The most dangerous direction  $\mathbf{d}_0$  is then the direction of the current space margin, which points from  $p$  to the center of the hazard sphere

$$\mathbf{d}_0 = \frac{\mathbf{r}_h - \mathbf{r}_p}{\|\mathbf{r}_h - \mathbf{r}_p\|} \quad (12)$$

or

$$\mathbf{d}_0 = \frac{\mathbf{r}_h^* - \mathbf{r}_p}{\|\mathbf{r}_h^* - \mathbf{r}_p\|} \quad (13)$$

in the multi-hazard scenario.

Note that there is no need to perform avoidance maneuvers when the system is far away from the hazard. Hence, we set an effective interval for the current space margin, i.e., only when  $d \in [\underline{\varepsilon}, \bar{\varepsilon}]$ , the system executes hazard avoidance control actions. The lower bound  $\underline{\varepsilon} > 0$  depends on the minimal distance that the system requires to turn around in the worst case, that is, approaching the hazard with full speed. The upper bound, on the other hand, reflects system sensitivity to the environment, as it determines when the system should apply avoidance maneuvers. As soon as the system enters the effective interval, a straightforward way of avoiding collision is to drag the system to the upper bound  $\bar{\varepsilon}$ . This maneuver becomes urgent as the current space margin  $d$  decreases. To this end, we set a safe target state  $\mathbf{x}_{safe}$  and realize hazard avoidance by steering the system towards the state. Define the safe target velocity as

$$\mathbf{v}_{safe} = -\frac{\underline{\varepsilon}}{d} v_{\max} \mathbf{d}_0 \quad (14)$$

where  $v_{\max}$  is the maximal allowable velocity during descent. When  $d = \underline{\varepsilon}$ ,  $\mathbf{v}_{safe} = -v_{\max} \mathbf{d}_0$ . The safe target position is set as

$$\mathbf{r}_{safe} = \mathbf{r}_h - \bar{\varepsilon} \mathbf{d}_0 \quad (15)$$

Then, we obtain the safe target state

$$\mathbf{x}_{safe} = [r_{safe}^x, r_{safe}^y, r_{safe}^z, v_{safe}^x, v_{safe}^y, v_{safe}^z]^T \quad (16)$$

and formulate a hazard avoidance performance index

$$J_h = \sum_{k=0}^{N-1} (\mathbf{x}(k) - \mathbf{x}_{safe})^T Q' (\mathbf{x}(k) - \mathbf{x}_{safe}) \quad (17)$$

Considering the effective interval of hazard avoidance, we set the weighting matrix as

$$Q' = \left(1 - \frac{d - \hat{\varepsilon}}{\sqrt{1 + (d - \hat{\varepsilon})^2}}\right) \mathbf{I}_6 \quad (18)$$

where  $\hat{\varepsilon} = (\bar{\varepsilon} + \underline{\varepsilon})/2$ .

By integrating the hazard avoidance performance index into model predictive control, we solve the following optimization problem on the receding horizon

$$\begin{aligned} \min & (\mathbf{x}(N) - \mathbf{x}_f)^T P (\mathbf{x}(N) - \mathbf{x}_f) + \sum_{k=0}^{N-1} [(\mathbf{x}(k) - \mathbf{x}_f)^T Q (\mathbf{x}(k) - \mathbf{x}_f) \\ & + (\mathbf{x}(k) - \mathbf{x}_{safe})^T Q' (\mathbf{x}(k) - \mathbf{x}_{safe}) + \mathbf{u}(k)^T R \mathbf{u}(k)] \\ \text{s.t.} & \quad \mathbf{x}(k+1) = \mathbf{A}_d \mathbf{x}(k) + \mathbf{B}_d \mathbf{u}(k) + \mathbf{C}_d \mathbf{g} \\ & \quad \mathbf{x}(0) = \mathbf{x}_0 = [r_0^T, v_0^T]^T, \\ & \quad \mathbf{x}(t_f) = \mathbf{x}_f = [r_f^T, v_f^T]^T, \\ & \quad \mathbf{x}(k) \in \mathcal{X}, \mathbf{u}(k) \in \mathcal{U}, \mathbf{x}(N) \in \mathcal{X}_f. \end{aligned} \quad (19)$$

where  $N$  is the length of the finite horizon, the weighting matrices  $Q, R$  are pre-selected constants, the terminal state weighting matrix  $P$  is calculated from

$$\mathbf{A}^T [P - P \mathbf{B} (\mathbf{B}^T P \mathbf{B} + R)^{-1} \mathbf{B}^T P] \mathbf{A} + Q - P = 0, \quad (20)$$

$\mathbf{x}_0$  is the current system state,  $\mathbf{x}_f$  is the desired terminal state, and  $\mathcal{X}_f \subset \mathcal{X}$  is the control invariant set of the system. The polyhedral invariant set  $\mathcal{X}_f$  is solved off-line on the basis of state feedback control Xi et al. (2009). By solving the above problem, the system applies only the first control action of the obtained optimal control sequence. Then, it recomputes the current space margin and the most dangerous direction, and updates the initial state. Whenever the system enters the effective interval of a nearby hazard, it temporarily alters its control objective from precise landing to hazard avoidance through an automatic tuning of the hazard avoidance performance index weight. By repetitively solving the optimization problem, the system drives itself along a physically feasible trajectory to the target landing site.

#### 4. SIMULATION

To verify the proposed method, we establish a Bennu-based asteroid landing scenario according to the OSIRIS-REx mission. Assume that the rotational speed  $\omega = 4.0679 \times 10^{-4}$  rad/s and the density of the asteroid  $\rho = 1.26 \times 10^3$  kg/m<sup>3</sup>. When the descent phase commences, the lander is at  $\mathbf{r}_0 = [100, -80, 380]^T$  m with an initial velocity  $\mathbf{v}_0 = [-1, 0, 0]^T$  m/s<sup>2</sup>. The target landing site is at  $\mathbf{r}_f = [-26, 0, 243]^T$  m and the desired terminal velocity is  $\mathbf{v}_f = [0, 0, 0]^T$  m/s. For simplicity, we employ a constant estimate error covariance during descent by setting

$$C_r = \begin{bmatrix} 16 & -2 & 0 \\ -2 & 16 & 1 \\ 0 & 1 & 9 \end{bmatrix}, C_v = \begin{bmatrix} 0.01 & -0.005 & -0.00012 \\ -0.005 & 0.0001 & 0.001 \\ -0.00012 & 0.001 & 0.09 \end{bmatrix}$$

The initial mean values of position estimate and velocity estimate are  $\boldsymbol{\mu}_r = [92.1505, -80.1792, 378.8226]^T$  m,  $\boldsymbol{\mu}_v = [-0.8596, -0.0022, -0.0855]^T$  m/s.

First, we determine the boundary of the actual system position from the  $3\sigma$  error ellipsoid, whose center is at  $\boldsymbol{\mu}_r$  and the lengths of the three semi-axes are 4 m, 4 m, 3 m respectively. According to Eq. (5), we take  $M_r = 50$  samples and obtain set  $\mathcal{S}_r$ . Then, we consider the range that the lander can reach in the position space when no control is applied in  $\Delta T = 3$  s. We sample  $M_v = 50$  points that follow  $N(\boldsymbol{\mu}_v, \boldsymbol{\sigma}_v)$  for prediction and obtain the uneven error ellipsoid set  $\mathcal{S}_E$  from Eq. (9).

In the simulated landing scenario, we set a semi-spherical hazard at  $\mathbf{r}_h = [14, -23, 250]^T$  m with a radius of  $R_h = 15$  m. In the uneven error ellipsoid set, we search for point  $p$  that is closest to the hazard and obtain the current space

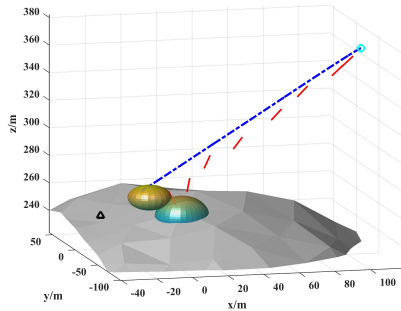


Fig. 2. Landing trajectory without hazard avoidance.

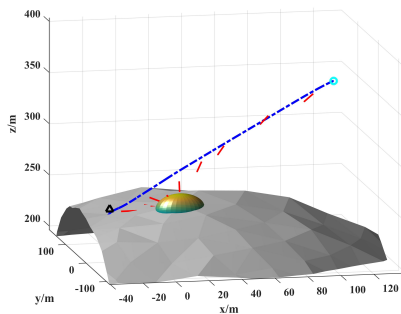


Fig. 3. Landing trajectory with hazard avoidance.

margin  $d = 133.9537\text{m}$  and the most dangerous direction  $\mathbf{d}_0 = [-0.4722, 0.3633, -0.8031]^T$  at the initial time. In model predictive control, we set the receding horizon length  $N = 8$ , the weighting matrices  $Q = \mathbf{I}_6, R = \mathbf{I}_3$ , the time step as 1.5 s, and use the YALMIP toolbox to solve the optimization problem.

For comparison, we first remove the hazard avoidance performance index from the optimization problem and compute the landing trajectory. In Fig. 2, the blue dotted line refers to the optimal trajectory and the red arrows are the most dangerous directions pointing from point  $p$  to the hazard center. The black triangle is the target landing site. The blue semi-sphere is the designed hazard and the yellow ellipsoid is the  $3\sigma$  position error ellipsoid at the termination time. As can be seen, the position error ellipsoid overlaps with the hazard and the landing process terminates prematurely. This indicates that the system predicts a potential collision with the hazard given the state estimates. For safety concerns, it stops and requires further hazard avoidance maneuvers. Then we incorporate the hazard avoidance performance index into trajectory optimization and set  $\bar{\varepsilon} = 20\text{m}, \underline{\varepsilon} = 2\text{m}$ . The generated trajectory is shown in Fig. 3. This time, the system keeps approaching the surface and the process terminates when the lander makes a touchdown in the neighborhood of the target landing site. No collision threat is predicted as the system keeps at least  $\underline{\varepsilon}$  away from the hazard.

## 5. CONCLUSION

In this paper, we propose an uneven error ellipsoid-based model predictive control for improving planetary landing safety under state uncertainties. Specifically, we consider the impact of position and velocity estimate errors and

quantify collision threats through computations of the current space margin and the most dangerous direction. By solving the trajectory optimization problem on a receding horizon, we generate a safe and physically feasible landing trajectory in a real-time manner. At last, we validate the method in a Bennu-based landing scenario and prove its effectiveness of guaranteeing system safety during descent.

## ACKNOWLEDGEMENTS

This work was supported by the National Key Research and Development Project (2019YFA0706500), the National Natural Science Foundation of China (61873302 and 61973032), the Basic Scientific Research Program of China (JCKY2018602B002JCKY2019602D022), and the Civil Aerospace Research Project of China.

## REFERENCES

- Cui, P., Qin, T., Zhu, S., Liu, Y., et al. (2018). Trajectory curvature guidance for Mars landings in hazardous terrains. *Automatica*, 93, 161–171.
- Dunham, D.W., Farquhar, R.W., McAdams, J.V., Holdridge, M., et al. (2002). Implementation of the first asteroid landing. *Icarus*, 159(2), 433–438.
- Ge, D., Cui, P., and Zhu, S. (2019). Recent development of autonomous gnc technologies for small celestial body descent and landing. *Progress in Aerospace Sciences*, 110, 100551.
- Jewison, C., Erwin, R.S., and Saenz-Otero, A. (2015). Model predictive control with ellipsoid obstacle constraints for spacecraft rendezvous. *IFAC Papers on Line*, 48(9), 257–262.
- Lee, U. and Mesbahi, M. (2017). Constrained autonomous precision landing via dual quaternions and model predictive control. *Journal of Guidance, Control, and Dynamics*, 40(2), 292–308.
- Liao-McPherson, D., Dunham, W.D., and Kolmanovsky, I. (2016). Model predictive control strategies for constrained soft landing on an asteroid. In *AIAA/AAS Astrodynamics Specialist Conference*, 5507.
- Lindner, M., Schiller, I., Kolb, A., and Koch, R. (2010). Time-of-flight sensor calibration for accurate range sensing. *Computer Vision and Image Understanding*, 114(12), 1318–1328.
- Park, H., Zagaris, C., Virgili-Llop, J., Zappulla, R., et al. (2016). Analysis and experimentation of model predictive control for spacecraft rendezvous and proximity operations with multiple obstacle avoidance. In *AIAA/AAS Astrodynamics Specialist Conference*, 5273.
- Reynolds, T. and Mesbahi, M. (2017). Small body precision landing via convex model predictive control. In *AIAA SPACE and Astronautics Forum and Exposition*.
- Szmuk, M., Acikmese, B., and Berning, A.W. (2016). Successive convexification for fuel-optimal powered landing with aerodynamic drag and non-convex constraints. In *AIAA Guidance, Navigation, and Control Conference*.
- Xi, Y., Zhu, H., and Li, D. (2009). Synthesizing off-line robust model predictive control based on polyhedron invariant set. *Control and Decision*, 24(2), 187–195.
- Yuan, X., Yu, Z., Cui, P., Xu, R., et al. (2018). Probability-based hazard avoidance guidance for planetary landing. *Acta Astronautica*, 144, 12–22.